Annals of Physics 391 (2018) 183–202

Contents lists available at ScienceDirect

Annals of Physics

journal homepage: www.elsevier.com/locate/aop

Polaron mobility obtained by a variational approach for lattice Fröhlich models

Milan Kornjača, Nenad Vukmirović *

Scientific Computing Laboratory, Center for the Study of Complex Systems, Institute of Physics Belgrade, University of Belgrade, Pregrevica 118, 11080 Belgrade, Serbia

ARTICLE INFO

Article history:
Received 28 September 2017
Accepted 27 January 2018
Available online 21 February 2018

Keywords:
Polaron
Mobility
Electron–phonon interaction
Fröhlich interaction
Kubo's formula

ABSTRACT

Charge carrier mobility for a class of lattice models with long-range electron–phonon interaction was investigated. The approach for mobility calculation is based on a suitably chosen unitary transformation of the model Hamiltonian which transforms it into the form where the remaining interaction part can be treated as a perturbation. Relevant spectral functions were then obtained using Matsubara Green's functions technique and charge carrier mobility was evaluated using Kubo's linear response formula. Numerical results were presented for a wide range of electron–phonon interaction strengths and temperatures in the case of one-dimensional version of the model. The results indicate that the mobility decreases with increasing temperature for all electron–phonon interaction strengths in the investigated range, while longer interaction range leads to more mobile carriers.

1. Introduction

There is a strong interest to understand the effects of electron–phonon interaction on electrical transport properties of semiconductors since it is the interaction mechanism that is present in every material being in most cases the dominant mechanism that limits the charge carrier mobility. In the case of semiconductors with wide bands and weak electron–phonon interaction (such as for example conventional inorganic semiconductors GaAs or Si), charge carrier mobility can be described using Bloch–Boltzmann theory [1–3] and it can be evaluated from electron–phonon scattering time and the effective mass of the carrier. Significant research efforts are currently devoted towards developing ab-initio methods for calculation of mobility in this regime [4–10] which is a non-trivial task due to the

* Corresponding author.
E-mail addresses: milan.kornjaca@ipb.ac.rs (M. Kornjača), nenad.vukmirovic@ipb.ac.rs (N. Vukmirović).

https://doi.org/10.1016/j.aop.2018.01.014
0003-4916/

necessity of taking a large number of points in the Brillouin zone to obtain accurate values of scattering times [11,12] and due to the difficulties of including long-range interaction with polar optical phonons within such approach [13,14]. In the opposite limit of narrow bands and strong electron–phonon interaction (which can be valid in some organic semiconductors based on small molecules) charge carrier transport is typically modeled using hopping theories [15], with hopping rates between the molecules evaluated using Marcus formula [16,17] or its generalizations [18–20], which consider only local electron–phonon interaction.

It is of significant importance to develop methods that can be used to evaluate charge carrier mobility beyond these two limiting regimes [21–24]. Due to difficulties in treating electron–phonon interaction of intermediate strength, the efforts to develop such methods are more scarce. These methods are usually based on a unitary transformation of the model Hamiltonian [25,26] and in practice these are applied to Hamiltonians with local electron–phonon interaction (Holstein model) [26,25] or short-range non-local interaction [27–29] (Peierls model). More recently, Quantum Monte Carlo techniques were also applied to evaluate the mobility in the Holstein and the Peierls model [30,31].

The main aim of this work is to develop a method for evaluating the mobility in systems with long-range electron–phonon interaction for a wide range of interaction strengths and temperatures. We consider a lattice model with long-range electron–phonon interaction of Fröhlich type and evaluate the mobility using an approach that combines unitary transformation of the Hamiltonian, Matsubara Green's function technique for evaluation of relevant spectral functions and Kubo's formula for calculation of mobility. The manuscript is organized as follows. In Section 2 we introduce the model Hamiltonian that is the subject of this work. In Section 3 we present the unitary transformation that is used to transform the Hamiltonian to the form where the remaining interaction can be treated using perturbative techniques, we derive the equations for optimal parameters of the unitary transformation and present numerical results for bandwidth renormalization. Equations for self-energies obtained using Matsubara Green's function technique are presented in Section 4 along with the numerical results for polaronic spectral functions. In Section 5 we present the derivation of mobility based on Kubo's linear response theory and numerical results for a wide range of temperatures and electron–phonon coupling strengths. Concluding remarks are given in Section 6.

2. Model Hamiltonian

We consider the following Hamiltonian that describes a periodic system of electrons and phonons that interact via long-range interaction:

$$H = -\sum_{\mathbf{m},\mathbf{n}} t_{\mathbf{m}-\mathbf{n}} c_{\mathbf{m}}^{\dagger} c_{\mathbf{n}} + \sum_{\mathbf{n}} \hbar\omega_0 b_{\mathbf{n}}^{\dagger} b_{\mathbf{n}} - \\ - \sum_{\mathbf{m},\mathbf{n}} \hbar\omega_0 f_{\mathbf{m}-\mathbf{n}} c_{\mathbf{n}}^{\dagger} c_{\mathbf{n}} (b_{\mathbf{m}}^{\dagger} + b_{\mathbf{m}}). \tag{1}$$

In Eq. (1) the vectors $\mathbf{m}$ and $\mathbf{n}$ label the sites of an infinite lattice, $c_{\mathbf{m}}$, $c_{\mathbf{m}}^{\dagger}$, $b_{\mathbf{m}}$, and $b_{\mathbf{m}}^{\dagger}$ are respectively annihilation and creation operators for electrons and phonons, $t_{\mathbf{m}-\mathbf{n}}$ is the electronic transfer integral that quantifies the electronic coupling between sites $\mathbf{m}$ and $\mathbf{n}$, $\hbar\omega_0$ is the energy of a phonon, while $f_{\mathbf{m}-\mathbf{n}}$ are dimensionless electron–phonon coupling parameters.

The Hamiltonian H considers a single electronic state per period of the system and a single dispersionless phonon band. While accurate modeling of real materials would certainly require a more elaborate Hamiltonian, we believe that it is essential first to address the properties of this relatively simple Hamiltonian. In the case when coupling parameters $f_{\mathbf{m}-\mathbf{n}}$ are zero except for $\mathbf{m} = \mathbf{n}$ the Hamiltonian reduces to a widely studied Holstein Hamiltonian [32]. In this work, we address a rather different scenario when $f_{\mathbf{m}-\mathbf{n}}$ is long-ranged.

Long-ranged electron–phonon interaction occurs as a consequence of interaction of electrons with a polarization field created from optical phonons in a polar material. To be more specific, an optical phonon at site $\mathbf{m}$ creates a dipole moment $\mathbf{p}_{\mathbf{m}} = p_{\mathbf{m}}\mathbf{e}_{\mathbf{m}}$, where $p_{\mathbf{m}}$ is its intensity and $\mathbf{e}_{\mathbf{m}}$ the unit vector in the direction of the dipole. Classical electrical potential at site $\mathbf{n}$ created by this dipole

is $V_{\mathbf{n},\mathbf{m}} = \frac{p_{\mathbf{m}}}{4\pi\varepsilon_0}\frac{\mathbf{e}_{\mathbf{m}}\cdot(\mathbf{n}-\mathbf{m})}{|\mathbf{n}-\mathbf{m}|^3}$. Since the dipole moment is proportional to phonon mode displacement $p_{\mathbf{m}} \propto \xi_{\mathbf{m}}$, we obtain $V_{\mathbf{n},\mathbf{m}} \propto \frac{\mathbf{e}_{\mathbf{m}}\cdot(\mathbf{n}-\mathbf{m})}{|\mathbf{n}-\mathbf{m}|^3}\xi_{\mathbf{m}}$. In the representation of second quantization this potential yields the term in the Hamiltonian of the form $-\sum_{\mathbf{m},\mathbf{n}}\frac{\mathbf{e}_{\mathbf{m}}\cdot(\mathbf{n}-\mathbf{m})}{|\mathbf{n}-\mathbf{m}|^3}c_{\mathbf{n}}^\dagger c_{\mathbf{n}}\left(b_{\mathbf{m}}+b_{\mathbf{m}}^\dagger\right)$ and consequently $f_{\mathbf{m}-\mathbf{n}} \propto \frac{\mathbf{e}_{\mathbf{m}}\cdot(\mathbf{n}-\mathbf{m})}{|\mathbf{n}-\mathbf{m}|^3}$. In the case of one dimensional model that will be the focus of our numerical study, the vectors $\mathbf{e}_{\mathbf{m}}$ and $\mathbf{n}-\mathbf{m}$ are collinear and the last expression reduces to $f_{\mathbf{m}-\mathbf{n}} \propto \frac{1}{|\mathbf{n}-\mathbf{m}|^2}$.

Previous derivation of the electron–phonon interaction parameter $f_{\mathbf{m}-\mathbf{n}}$ is meaningful for $\mathbf{m} \neq \mathbf{n}$. To include local electron–phonon interaction, one has to introduce an additional parameter describing its strength. Thus, the final form of the interaction coefficients that will be used in our study is:

$$f_{\mathbf{m}-\mathbf{n}} = \alpha_1\delta_{\mathbf{m},\mathbf{n}} + \frac{\alpha_2 C^2}{|\mathbf{m}-\mathbf{n}|^2}(1-\delta_{\mathbf{m},\mathbf{n}}), \tag{2}$$

where C is the lattice constant, while α_1 and α_2 are dimensionless electron–phonon coupling constants arising respectively from local and long-range non-local electron–phonon interaction.

It is useful to redefine the couplings to have one coupling constant that determines overall interaction strength and the other that describes the relative strength of interaction with the central atom and all the other atoms, i.e. the electron–phonon interaction range. It can be done in multiple ways, but here the procedure which was used in Ref. [33] for a different 1D lattice Fröhlich Hamiltonian will be loosely followed. As a measure of the interaction strength, the binding energy of the polaron in the strong-coupling limit is used. This binding energy is given as

$$\frac{E_b}{\hbar\omega_0} = \sum_{\mathbf{m}} f_{\mathbf{m}}^2 = \alpha_1^2 + \kappa\alpha_2^2, \tag{3}$$

where $\kappa = 2\sum_{j=1}^{\infty}\frac{1}{j^4} = \frac{\pi^4}{45}$. We then redefine the coupling constants as $\alpha_1 = \alpha\cos\psi$ and $\alpha_2 = \frac{1}{\sqrt{\kappa}}\alpha\sin\psi$. The binding energy in the strong-coupling limit then becomes $\frac{E_b}{\hbar\omega_0} = \alpha^2$ and therefore the parameter α is a measure of electron–phonon interaction strength. On the other hand, the parameter ψ is a measure of electron–phonon interaction range. The case of $\psi = 0$ corresponds to the purely local Holstein Hamiltonian, while in the opposite extreme, $\psi = \frac{\pi}{2}$, the interaction with the central molecule is nonexistent. However, it is not expected that interaction of an electron with a phonon on the neighboring site could be stronger than its interaction with the phonon on the same site. Therefore, the upper limit on the sensible values of ψ is $\psi \approx \frac{\pi}{3}$ when the coefficients f_0 and f_1 become equal.

3. Unitary transformation of the Hamiltonian

Our general strategy used to address the carrier transport properties in the model studied is based on unitary transformation of the Hamiltonian to the form where it consists of noninteracting polaron part, noninteracting phonon part and the part describing residual polaron–phonon interaction. Parameters of the transformation will be chosen to make the residual polaron–phonon interaction as small as possible, so that it can be treated using perturbative techniques.

In the case of strong coupling when electron–phonon interaction is much stronger than the electronic coupling, the Hamiltonian can be exactly diagonalized using the Lang–Firsov [34] transformation

$$\tilde{H} = e^{-S}He^{S} \tag{4}$$

with

$$S = \frac{1}{\sqrt{N}}\sum_{\mathbf{m},\mathbf{n}} f_{\mathbf{m}-\mathbf{n}}c_{\mathbf{n}}^\dagger c_{\mathbf{n}}(b_{\mathbf{m}}^\dagger - b_{\mathbf{m}}). \tag{5}$$

On the other hand, in the case of weak coupling, no unitary transformation is needed since the perturbation techniques are directly applicable. To include this fact in a single transformation that aims

to describe polarons in various coupling regimes, we make Lang–Firsov transformation dependent on a set of variational parameters ($D_{\mathbf{m}-\mathbf{n}}$), so that it takes the form:

$$S = \frac{1}{\sqrt{N}} \sum_{\mathbf{m},\mathbf{n}} D_{\mathbf{m}-\mathbf{n}} c_{\mathbf{n}}^{\dagger} c_{\mathbf{n}} (b_{\mathbf{m}}^{\dagger} - b_{\mathbf{m}}). \tag{6}$$

We will further assume for simplicity that the system exhibits inversion symmetry. In addition, since we are interested to obtain the mobility in the limit of low carrier concentration we will project the transformed Hamiltonian to the part of Hilbert space spanned by single particle excitations. The transformed Hamiltonian then takes the form

$$\tilde{H}(\mathbf{D}) = H_0(\mathbf{D}) + V_1(\mathbf{D}) + V_2(\mathbf{D}), \tag{7}$$

where its noninteracting part H_0 is given as

$$H_0 = \sum_{\mathbf{k}} c_{\mathbf{k}}^{\dagger} c_{\mathbf{k}} E_{\mathbf{k}} + \sum_{\mathbf{q}} \hbar\omega_0 b_{\mathbf{q}}^{\dagger} b_{\mathbf{q}} \tag{8}$$

with

$$E_{\mathbf{k}} = -\sum_{\mathbf{R}^+} J_{\mathbf{R}}(\mathbf{D}) \cos \mathbf{k}\mathbf{R} + \sum_{\mathbf{q}} \hbar\omega_0 (D_{\mathbf{q}}^2 - 2 f_{\mathbf{q}} D_{\mathbf{q}}) \tag{9}$$

and

$$J_{\mathbf{R}}(\mathbf{D}) = 2 t_{\mathbf{R}} e^{-\sum_{\mathbf{q}} D_{\mathbf{q}}^2 (1-\cos \mathbf{q}\mathbf{R})(2n_0+1)}, \tag{10}$$

while interacting parts V_1 and V_2 read

$$V_1 = -\sum_{\mathbf{k},\mathbf{q}} \hbar\omega_0 (f_{\mathbf{q}} - D_{\mathbf{q}}) c_{\mathbf{k}-\mathbf{q}}^{\dagger} c_{\mathbf{k}} (b_{\mathbf{q}}^{\dagger} + b_{-\mathbf{q}}) \tag{11}$$

and

$$V_2 = -\sum_{\mathbf{k}_1,\mathbf{k}_2} \left[\frac{1}{N} \sum_{\mathbf{m},\mathbf{n}} t_{\mathbf{m}-\mathbf{n}} (\theta_{\mathbf{m}}^{\dagger} \theta_{\mathbf{n}} - \langle \theta_{\mathbf{m}}^{\dagger} \theta_{\mathbf{n}} \rangle_0) \times \right. \\ \left. \times e^{i(\mathbf{k}_1 \mathbf{m} - \mathbf{k}_2 \mathbf{n})} \right] c_{\mathbf{k}_1}^{\dagger} c_{\mathbf{k}_2}. \tag{12}$$

In Eqs. (8)–(12) the summations over $\mathbf{k}$ and $\mathbf{q}$ wave vectors are performed over the first Brillouin zone. The operators $c_{\mathbf{k}}$ and $b_{\mathbf{q}}$ and the numbers $f_{\mathbf{q}}$ and $D_{\mathbf{q}}$ denote respectively Fourier transforms of $c_{\mathbf{n}}$, $b_{\mathbf{n}}$, $f_{\mathbf{n}}$ and $D_{\mathbf{n}}$ defined as

$$c_{\mathbf{k}} = \frac{1}{\sqrt{N}} \sum_{\mathbf{n}} c_{\mathbf{n}} e^{i\mathbf{k}\mathbf{n}}, \tag{13}$$

and similarly for $b_{\mathbf{q}}$, $f_{\mathbf{q}}$ and $D_{\mathbf{q}}$. N is the number of lattice sites, while the symbol $\sum_{\mathbf{R}^+}$ in Eq. (9) denotes the summation over one half of the crystal lattice vectors (the other half are space-inversion images of the selected ones). The mean number of phonons in equilibrium at a temperature T in phonon mode of energy $\hbar\omega_0$ is denoted as $n_0 = \left(e^{\frac{\hbar\omega_0}{k_B T}} - 1 \right)^{-1}$. The operators $\theta_{\mathbf{m}}$ are defined as

$$\theta_{\mathbf{m}} = e^{\sum_{\mathbf{q}} D_{\mathbf{q}} (b_{\mathbf{q}}^{\dagger} - b_{-\mathbf{q}}) e^{i\mathbf{q}\mathbf{m}}} \tag{14}$$

and $\langle \theta_{\mathbf{m}}^{\dagger} \theta_{\mathbf{n}} \rangle_0$ denotes the average over the noninteracting phonon part of the Hamiltonian which reads

$$\theta_{\mathbf{m}-\mathbf{n}}^0 = \langle \theta_{\mathbf{m}}^{\dagger} \theta_{\mathbf{n}} \rangle_0 = e^{-\frac{1}{2} \sum_{\mathbf{q}} D_{\mathbf{q}}^2 \left| e^{i\mathbf{q}\mathbf{n}} - e^{i\mathbf{q}\mathbf{m}} \right|^2 (2n_0+1)}. \tag{15}$$

To find the optimal variational parameters $\mathbf{D}$, we exploit Bogoliubov inequality [35] for free energy F

$$\begin{aligned} F\left(\tilde{H}\right) &= -\frac{1}{\beta}\ln \mathrm{Tr}\left(e^{-\beta\tilde{H}}\right) \\ &\leq -\frac{1}{\beta}\ln \mathrm{Tr}\left(e^{-\beta H_0}\right) + \langle \tilde{H} - H_0\rangle_{H_0}, \end{aligned} \tag{16}$$

where $\langle \ldots \rangle_{H_0}$ denotes averaging with respect to the Hamiltonian H_0 and $\beta = \frac{1}{k_B T}$. Since in our case thermodynamical averages over phononic degrees of freedom yield $\langle V_1 + V_2\rangle_{H_0} = 0$, Eq. (16) reduces to

$$F\left(\tilde{H}\right) \leq -\frac{1}{\beta}\ln \mathrm{Tr}\left(e^{-\beta H_0}\right). \tag{17}$$

Evaluation of the expression on the right hand side of Eq. (17) is straightforward because H_0 is diagonal. To obtain the optimal unitary transformation, we minimize the value of this expression with respect to variational parameters $D_{\mathbf{q}}$. When this expression is minimized, upper bound on free energy of the system is closest to true free energy. It is therefore expected that at the same time, the effect of nondiagonal terms $V_1 + V_2$ will be smallest so that these can be treated using perturbative techniques.

To minimize the expression on the right hand side of Eq. (17), phononic part of the trace will be omitted since it does not depend on variational coefficients. The expression for polaronic part is:

$$\mathcal{F}^{\mathrm{pl}}(\mathbf{D}) = -\frac{1}{\beta}\ln\sum_{\mathbf{k}} e^{-\beta E_{\mathbf{k}}}, \tag{18}$$

Parameters of the optimal unitary transformation are obtained by solving the system of equations obtained from the condition $\frac{\partial \mathcal{F}^{\mathrm{pl}}}{\partial D_{\mathbf{q}}} = 0$.

This system of equations can be reduced to a single nonlinear equation in the case of three dimensional cubic lattice with nearest neighbor coupling. Namely, by exploiting the cubic symmetry one obtains

$$J_{\mathbf{C}_x}(\mathbf{D}) = J_{\mathbf{C}_y}(\mathbf{D}) = J_{\mathbf{C}_z}(\mathbf{D}) = J_{\mathbf{C}}(\mathbf{D}), \tag{19}$$

where $\mathbf{C}_x$, $\mathbf{C}_y$ and $\mathbf{C}_z$ are lattice vectors of three nearest neighbors in positive directions of x, y and z axes, respectively. The equations for variational parameters then read

$$D_{\mathbf{q}} = \frac{f_q}{1 + \frac{I_1(\beta J_{\mathbf{C}}(\mathbf{D}))}{I_0(\beta J_{\mathbf{C}}(\mathbf{D}))}\frac{J_{\mathbf{C}}(\mathbf{D})}{\hbar\omega_0}(2n_0+1)\sum_{i=x,y,z}(1-\cos\mathbf{q}\mathbf{C}_i)}, \tag{20}$$

where I_n denotes modified Bessel function of the first kind of order n. After performing a substitution of the expression (20) into the expression (10) that reads in this case

$$J_{\mathbf{C}}(\mathbf{D}) = 2t_{\mathbf{C}} e^{-\sum_{\mathbf{q}} D_{\mathbf{q}}^2 (1-\cos\mathbf{q}\mathbf{C})(2n_0+1)}, \tag{21}$$

we obtain the nonlinear equation with a single unknown variable $J_{\mathbf{C}}(\mathbf{D})$. In the case of an one dimensional model, the expressions (20) and (21) still hold, with a difference that the sum $\sum_{i=x,y,z}$ in Eq. (20) should be replaced by $\sum_{i=x}$. It was checked that the solution of Eqs. (20)–(21) exhibits expected behavior for weak and strong coupling. Namely, for weak interaction when $f_{\mathbf{q}} \to 0$, we obtain $D_{\mathbf{q}} \to 0$, so that the unitary transformation is close to unity. For strong interaction, $J_{\mathbf{C}}(\mathbf{D}) \to 0$, implying $D_{\mathbf{q}} \to f_{\mathbf{q}}$, which corresponds to usual Lang–Firsov transformation.

Next, we discuss the features of the numerical solution of Eqs. (20)–(21). The dependence of band narrowing factor $\frac{J_{\mathbf{C}}}{2t_{\mathbf{C}}}$ on coupling strength and temperature for several values of transfer integral and for two different values of electron–phonon interaction range is presented in Fig. 1. Depending on the values of $\frac{t_{\mathbf{C}}}{\hbar\omega_0}$ and ψ two distinct cases emerge when we solve Eqs. (20)–(21). In the first case, a single solution exists for all values of temperature and coupling constant. Then, the values of renormalized

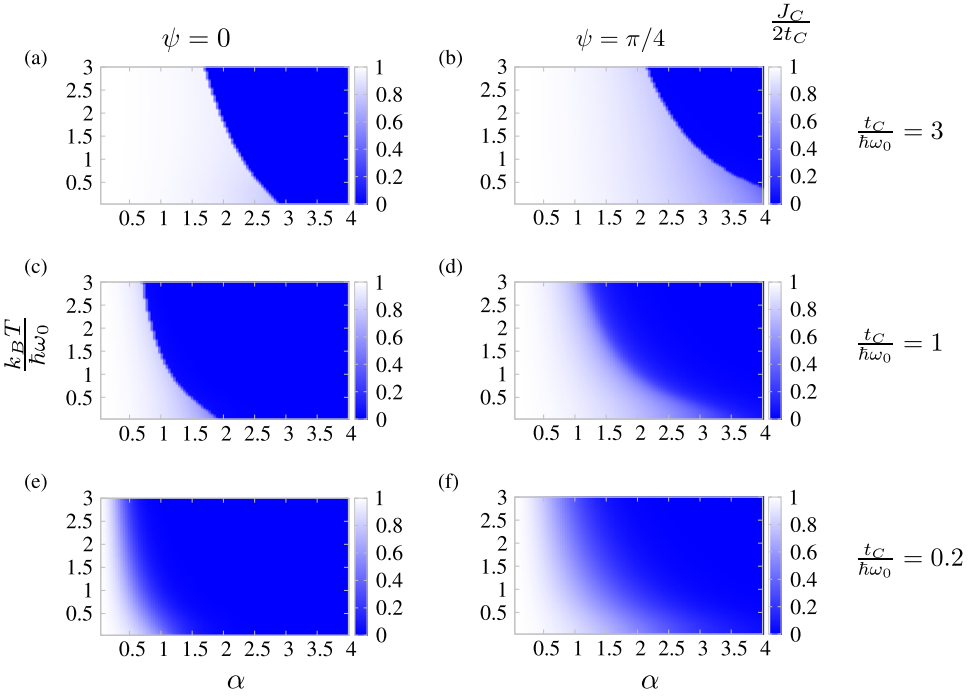

Fig. 1. Dependence of bandwidth narrowing factor $\frac{J_C}{2t_C}$ on coupling strength α and temperature k_BT. The dependence is shown for (a) $\frac{t_C}{\hbar\omega_0} = 3, \psi = 0$; (b) $\frac{t_C}{\hbar\omega_0} = 3, \psi = \pi/4$; (c) $\frac{t_C}{\hbar\omega_0} = 1, \psi = 0$; (d) $\frac{t_C}{\hbar\omega_0} = 1, \psi = \pi/4$; (e) $\frac{t_C}{\hbar\omega_0} = 0.2, \psi = 0$; (f) $\frac{t_C}{\hbar\omega_0} = 0.2, \psi = \pi/4$.

bandwidth vary smoothly in the whole parameter range, see for example parts (d)–(f) of Fig. 1. In the second case there are two solutions of Eqs. (20)–(21). One of these solution exists only for relatively weak interaction strength and the other for relatively strong, while there is a range of interaction strengths where these solutions coexist. In this case, we choose the solution with lower free energy. As a consequence of presence of multiple solutions, calculated renormalized bandwidth does not vary smoothly with the change of coupling strength and temperature. It exhibits a sharp transition at some point, see for example parts (a)–(c) of Fig. 1. We find generally that the first case occurs for $\frac{t_C}{\hbar\omega_0} < 1$ regardless of interaction range. The second case exists often when $\frac{t_C}{\hbar\omega_0} > 1$ but the sharpness and existence of the transition depend on the temperature and nature of the Hamiltonian. For short-range interaction ($\psi = 0$) the transition is sharp, while for larger ψ the transition becomes less sharp and even vanishes for lower temperatures. It must be emphasized that the apparent sharp transition is the consequence of the method used, since the free energy functional is only the upper bound to the real free energy of the system. It has been rigorously proven that free energy is a smooth function of coupling constant for a wide class of Hamiltonians with electron–phonon interaction [36–38].

From Fig. 1 we also see that short-range interaction is more efficient in narrowing the band. This effect was previously reported in Quantum Monte Carlo calculations for a different one dimensional lattice polaron Hamiltonian class [39]. In our case, it can be understood from Eq. (21). For stronger interaction $D_{\mathbf{q}} \to f_{\mathbf{q}}$ and the bandwidth is determined by the factor in the exponent $\sum_{\mathbf{q}} f_{\mathbf{q}}^2(1 - \cos \mathbf{qC})(2n_0 + 1)$. This factor is smaller for long-range interaction because of the different momentum dependence of interaction coefficients $f_{\mathbf{q}}$. This dependence is shown in Fig. 2 for several values of interaction range ψ. Longer range interaction is the strongest for small momenta, however, the factor $1 - \cos \mathbf{qC}$ suppresses its effect for small momenta. As a consequence, momentum independent short-range interaction becomes more effective. We also note that in addition to the maximum at $q = 0$ the

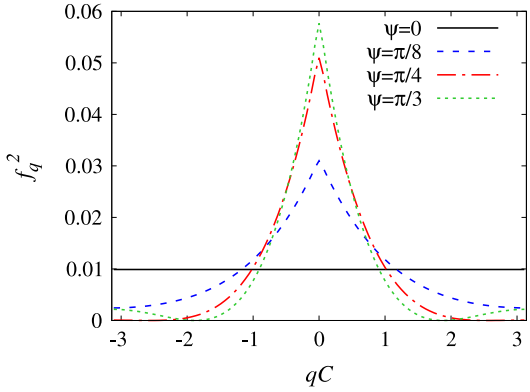

Fig. 2. Momentum dependence of the square of interaction coefficients f_q for $\alpha = 1$ and several values of electron–phonon interaction range ψ in the case of an one dimensional model.

function f_q^2 exhibits another less pronounced maximum at $qC = \pm\pi$ for $\psi = \pi/3$. This maximum is even more pronounced when $\psi > \pi/3$ and occurs due to the fact that interaction with first neighbor is comparable or stronger than local interaction. Since such a situation is not physical, we have restricted our analysis to the cases when $\psi \leq \pi/3$.

We note that qualitatively the same behavior of variational parameters and bandwidth narrowing factor would be obtained also in higher dimensional models.

4. Spectral properties

In this section we present the results of the calculation of relevant Green's functions, self-energies and corresponding spectral functions which will be needed for evaluation of mobility. In Hamiltonian $\tilde{H}$ we treat the term $V = V_1 + V_2$ as a perturbation. We employ the Matsubara Green's function technique [40] and expand the Green's function up to terms of second order in interaction V. After obtaining the analytical expressions for Matsubara Green's functions on imaginary frequency axis, we perform analytical continuation to real frequency axis and obtain the expressions that relate the retarded Green's function and corresponding retarded self-energy. We also employ the self-consistent Born approximation [40,41] by replacing the bare Green's functions with a dressed one in these expressions. The expressions for retarded self-energy then read:

$$\Sigma^R_{\mathbf{k}}(\omega) = \Sigma^{(0)}_{\mathbf{k}}(\omega) + \Sigma^{(1)}_{\mathbf{k}}(\omega) + \Sigma^{(2)}_{\mathbf{k}}(\omega), \tag{22}$$

where

$$\Sigma^{(0)}_{\mathbf{k}}(\omega) = \sum_{\mathbf{q}} \omega_0^2 (f_{\mathbf{q}} - D_{\mathbf{q}})^2 \left[(n_0+1) G^R_{\mathbf{k}-\mathbf{q}}(\omega - \omega_0) + n_0 G^R_{\mathbf{k}-\mathbf{q}}(\omega + \omega_0) \right], \tag{23}$$

$$\Sigma^{(1)}_{\mathbf{k}}(\omega) = -\frac{1}{\hbar} \sum_{\mathbf{q}} \omega_0 \left(f_{\mathbf{q}} - D_{\mathbf{q}}\right) D_{\mathbf{q}} \times \left[(n_0+1) G^R_{\mathbf{k}-\mathbf{q}}(\omega - \omega_0) - n_0 G^R_{\mathbf{k}-\mathbf{q}}(\omega + \omega_0) \right] \times \sum_{\mathbf{X}} t_{\mathbf{X}} \theta^0_{\mathbf{X}} \left(e^{i\mathbf{k}\mathbf{X}} - e^{-i(\mathbf{k}-\mathbf{q})\mathbf{X}}\right) \left(1 - e^{-i\mathbf{q}\mathbf{X}}\right), \tag{24}$$

$$\Sigma^{(2)}_{\mathbf{k}}(\omega) = \frac{i}{N\hbar^2} \sum_{\mathbf{q}} \int_{-\infty}^{\infty} \mathrm{d}t \; e^{i\omega t} D^{>(2)}_{\mathbf{k}-\mathbf{q},\mathbf{k},-\mathbf{q}}(t) G^R_{\mathbf{k}-\mathbf{q}}(t). \tag{25}$$

The quantities that appear in Eqs. (23)–(25) have the following meaning. The retarded Green's function in the time domain is defined as

$$G^R_{\mathbf{k}}(t) = -i\Theta(t)\langle c_{\mathbf{k}}(t)c^\dagger_{\mathbf{k}} + c^\dagger_{\mathbf{k}}c_{\mathbf{k}}(t)\rangle, \tag{26}$$

where $\Theta(t)$ denotes the Heaviside step function and $\langle \ldots \rangle$ denotes the grand canonical ensemble average with respect to $\tilde{H}$, while $c_{\mathbf{k}}(t)$ are electron annihilation operators in Heisenberg picture. Green's function in frequency domain is related to Green's function in time domain via $G^R_{\mathbf{k}}(\omega) = \int_{-\infty}^{\infty} \mathrm{d}t\, e^{i\omega t} G^R_{\mathbf{k}}(t)$. The function $D^{>(2)}_{\mathbf{k}',\mathbf{k}'',\mathbf{q}'}(t)$ reads

$$\begin{aligned} D^{>(2)}_{\mathbf{k}',\mathbf{k}'',\mathbf{q}'}(t) = -i \sum_{\mathbf{X},\mathbf{Y},\mathbf{Z}} t_{\mathbf{X}} t_{\mathbf{Y}} \theta^0_{\mathbf{X}} \theta^0_{\mathbf{Y}} e^{i(\mathbf{k}'\mathbf{X}+\mathbf{k}''\mathbf{Y}-\mathbf{q}'\mathbf{Z})} \times \\ \times \left[\theta_{\mathbf{X},\mathbf{Y},\mathbf{Z}}(t) - 1\right], \end{aligned} \tag{27}$$

where

$$\begin{aligned} \theta_{\mathbf{X},\mathbf{Y},\mathbf{Z}}(t) = \exp\left\{ - \sum_{\mathbf{q}} D^2_{\mathbf{q}} \left[(n_0+1)e^{-i\omega_0 t} + n_0 e^{i\omega_0 t}\right] \times \right. \\ \left. \left(1 - e^{-i\mathbf{q}\mathbf{X}}\right)\left(1 - e^{i\mathbf{q}\mathbf{Y}}\right) e^{i\mathbf{q}\mathbf{Z}} \right\}. \end{aligned} \tag{28}$$

Eqs. (22)–(25) and the Dyson equation

$$G^R_{\mathbf{k}}(\omega) = \frac{G^{R(0)}_{\mathbf{k}}(\omega)}{1 - \Sigma^R_{\mathbf{k}}(\omega) G^{R(0)}_{\mathbf{k}}(\omega)}, \tag{29}$$

where $G^{R(0)}_{\mathbf{k}}(\omega) = \lim_{\delta\to 0^+} \frac{1}{\omega - \frac{E_{\mathbf{k}} - E_F}{\hbar} + i\delta}$ is the Green's function of noninteracting system (where E_F is the chemical potential), form the system of equations that is solved self-consistently to obtain the retarded Green's function and the corresponding spectral function $A_{\mathbf{k}}(\omega) = -2 \cdot \mathrm{Im}[G^R_{\mathbf{k}}(\omega)]$.

Numerical calculations were performed for an one dimensional model with $N = 100$ lattice sites. It has been found that increasing the number of sites changes the mobility negligibly. The number of points used for discretization in time, or equivalently, frequency domain was $2^{13} = 8192$. The range of frequencies was tuned such that all the relevant energies are included in calculation. This range is determined by the phononic factor $D^{>(2)}$ which is needed for self-energy and thus Green's function calculation. This factor contains Fourier components in multiples of $\hbar\omega_0$. The strongest Fourier component scales with interaction strength and temperature as $\alpha^2 n_0$. The frequencies four times higher than that of the main Fourier component of $D^{>(2)}$ were included in the calculation. It turns out that it is most challenging to perform the calculation for very weak coupling when spectral lines are narrow. Fortunately, in these cases one can use analytical results for the weak coupling case. Numerical results are shown only for parameters sets where spectral widths are wide enough that the spectral functions can be reliably represented.

Spectral functions obtained from our calculations when $\psi = \frac{\pi}{4}$ and $\frac{k_B T}{\hbar\omega_0} = 0.4$ for two different values of $\frac{t_{\mathbf{C}}}{\hbar\omega_0}$ are presented in Figs. 3 and 4. In the $\frac{t_{\mathbf{C}}}{\hbar\omega_0} = 0.2$ case, the spectral function varies smoothly and band narrowing is gradual, as could have been expected also from the results for band narrowing factor in Section 3. For large interaction strength the band becomes almost flat. Upon closer inspection, one can also notice the appearance of one or more bands separated by multiples of ω_0 from the main band. The bands are consequences of single-phonon and multi-phonon scatterings and as such their spectral weight and number increases with increase of coupling strength.

In the case when bandwidth is significantly larger than the phonon energy, a richer behavior is observed, see Fig. 4 for the case $\frac{t_{\mathbf{C}}}{\hbar\omega_0} = 3$. The first feature that arises is the band splitting at ω_0 above the band minimum. With increasing the coupling strength, additional splittings arise and thus a sequence of bands each at the distance ω_0 forms, with the lowest one being more and more prominent. These results complement a simplified picture that one might acquire from the interpretation of results of Section 3, in which a single band of almost unrenormalized bandwidth exists until the

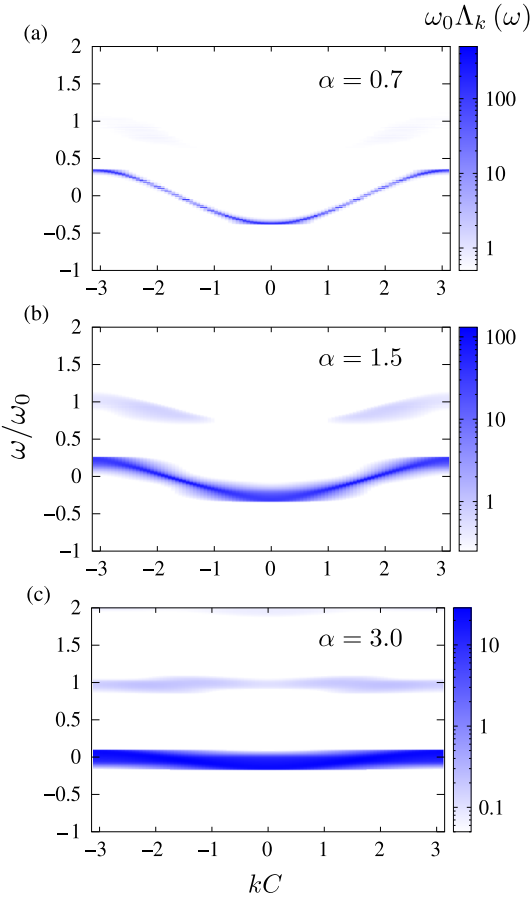

Fig. 3. Polaronic spectral function for different coupling strengths and $\frac{t_C}{\hbar\omega_0} = 0.2$, $\psi = \frac{\pi}{4}$ and $\frac{k_B T}{\hbar\omega_0} = 0.4$.

sharp transition after which one very narrow band arises. The change of spectrum in fact arises in a smoother way — by splitting the initial band into a number of narrower ones which are at the end each strongly narrowed. A similar picture was obtained in previous calculations of spectra for the Holstein model [42].

In Fig. 4 one additional interesting feature may be seen. At coupling strengths close to the strength at which the band strongly narrows, the band minimum appears at momentum different from zero. Such a feature has been previously observed in the case of Peierls Hamiltonian with short-range non-local electron–phonon interaction treated using self-consistent Born approximation and more exact treatments [41]. As pointed out in Ref. [41], such an effect is expected to happen when non-locality of electron–phonon interaction increases. We confirm such a behavior as we notice that the effect is more prominent for larger ψ.

5. Carrier mobility

To evaluate DC charge carrier mobility in the limit of low electric fields and low carrier concentration we apply the Kubo's linear response formula in the form [40,25]

$$\mu_{xx} = \frac{\beta}{2N_c e_0} \int_{-\infty}^{\infty} \mathrm{d}t \langle j_x(t) j_x(0) \rangle_H. \tag{30}$$

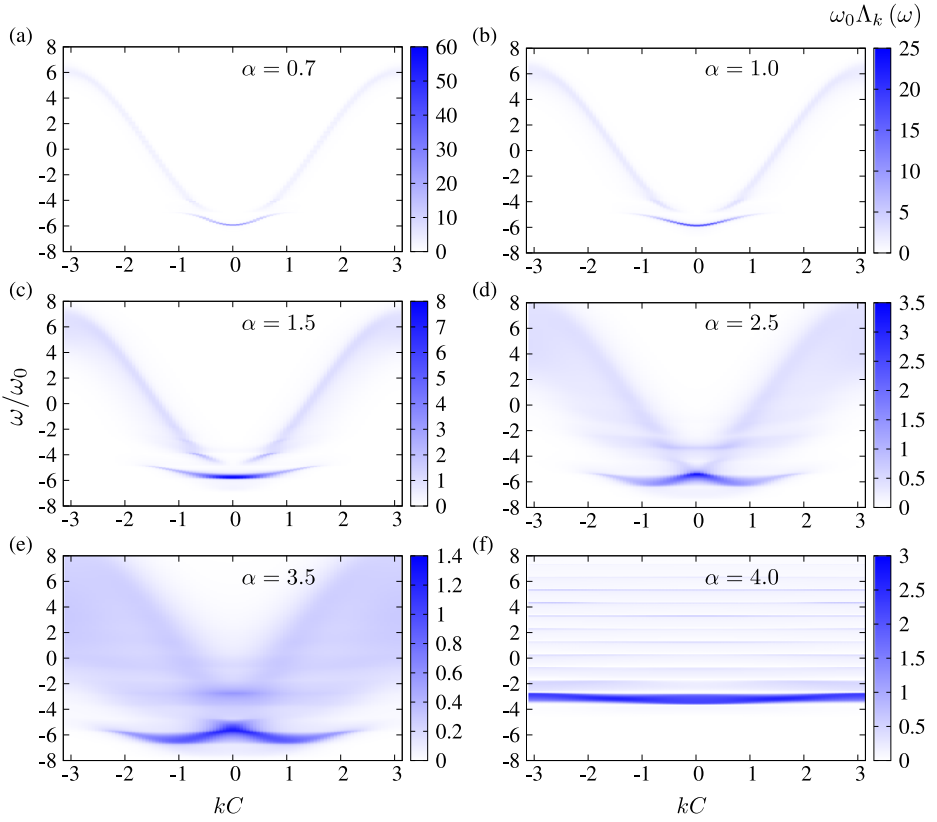

Fig. 4. Polaronic spectral function for different coupling strengths and $\frac{t_C}{\hbar\omega_0} = 3.0$, $\psi = \frac{\pi}{4}$ and $\frac{k_B T}{\hbar\omega_0} = 0.4$.

In Eq. (30) μ_{xx} denotes the xx-component of the mobility tensor, N_c is total number of charge carriers in the system, e_0 is the absolute value of electron charge, while j_x is the x-component of the operator

$$\mathbf{j} = \frac{e_0}{i\hbar} \sum_{\mathbf{m},\mathbf{n}} (\mathbf{m} - \mathbf{n}) t_{\mathbf{m}-\mathbf{n}} c^\dagger_{\mathbf{m}} c_{\mathbf{n}}. \tag{31}$$

The subscript H is introduced to denote both that $\langle \ldots \rangle_H$ denotes averaging with respect to H and that $j_x(t)$ is the operator in Heisenberg picture with respect to Hamiltonian H.

To evaluate the expression (30), it is more convenient to transform it to the form which involves the Hamiltonian $\tilde{H}$ and then perform the perturbative expansion. We therefore exploit the identity [27]

$$\langle j_a(t) j_b(0) \rangle_H = \left\langle \tilde{j}_a(t) \tilde{j}_b(0) \right\rangle_{\tilde{H}}, \tag{32}$$

where $\tilde{\mathbf{j}} = e^{-S} \mathbf{j} e^{S}$ and reads

$$\tilde{\mathbf{j}} = \sum_{\mathbf{k},\mathbf{q},\mathbf{q}'} \mathbf{J}_{\mathbf{k}} c^\dagger_{\mathbf{q}} c_{\mathbf{q}'} \theta^\dagger_{\mathbf{k}-\mathbf{q}} \theta_{\mathbf{k}-\mathbf{q}'}, \tag{33}$$

with

$$\mathbf{J}_{\mathbf{k}} = \frac{e_0}{i\hbar} \sum_{\mathbf{R}} \mathbf{R}\, t_{\mathbf{R}} e^{i\mathbf{k}\mathbf{R}} \tag{34}$$

and

$$\theta_{\mathbf{k}} = \frac{1}{N}\sum_{\mathbf{R}} \theta_{\mathbf{R}} e^{i\mathbf{k}\mathbf{R}}. \tag{35}$$

The mobility then reads:

$$\begin{aligned}\mu_{xx} =& \frac{\beta}{2N_c e_0}\sum_{\mathbf{k},\mathbf{q}}\sum_{\mathbf{k}',\mathbf{q}'}\sum_{\mathbf{k}'',\mathbf{q}''}\int_{-\infty}^{\infty} \mathrm{d}t (J_{\mathbf{k}})_x (J_{\mathbf{q}})_x \times \\ &\times \langle c^{\dagger}_{\mathbf{k}'}(t) c_{\mathbf{q}'}(t) \theta^{\dagger}_{\mathbf{k}-\mathbf{k}'}(t) \theta_{\mathbf{k}-\mathbf{q}'}(t) c^{\dagger}_{\mathbf{k}''} c_{\mathbf{q}''} \theta^{\dagger}_{\mathbf{q}-\mathbf{k}''} \theta_{\mathbf{q}-\mathbf{q}''} \rangle_{\tilde{H}}.\end{aligned} \tag{36}$$

We have resorted to calculation of μ_{xx} component of mobility tensor since this is the only component in the case of one-dimensional system, while the mobility tensor is reduced to a scalar in principal directions basis in the case of three dimensional cubic lattice. Next, we evaluate the first non-zero term in the perturbative expansion of μ_{xx} where H_0 is the noninteracting Hamiltonian and $\tilde{H} - H_0 = V_1 + V_2$ the interaction. It turns out that the zeroth term in the expansion gives a nontrivial contribution to μ_{xx}. This term is obtained by replacing $\tilde{H}$ with H_0 in Eq. (36). It is evaluated by performing the average over the terms involving products of phononic operators using the identity

$$\left\langle \theta^{\dagger}_{\mathbf{m}}(t)\theta_{\mathbf{n}}(t)\theta^{\dagger}_{\mathbf{l}}\theta_{\mathbf{j}} \right\rangle_{H_0} = \theta^0_{\mathbf{m}-\mathbf{n}}\theta^0_{\mathbf{l}-\mathbf{j}}\theta_{\mathbf{m}-\mathbf{n},\mathbf{l}-\mathbf{j},\mathbf{m}-\mathbf{l}}(t) \tag{37}$$

and exploiting the fact that

$$\begin{aligned}&\left\langle c^{\dagger}_{\mathbf{k}'}(t) c_{\mathbf{q}'}(t)\, c^{\dagger}_{\mathbf{k}''} c_{\mathbf{q}''} \right\rangle_{H_0} = \\ &\qquad = \delta_{\mathbf{k}',\mathbf{q}''}\delta_{\mathbf{q}',\mathbf{k}''} \left\langle c^{\dagger}_{\mathbf{k}'}(t) c_{\mathbf{q}''} \right\rangle_{H_0} \left\langle c_{\mathbf{q}'}(t) c^{\dagger}_{\mathbf{k}''} \right\rangle_{H_0},\end{aligned} \tag{38}$$

where the term involving the square of the number of carriers was excluded in the last equation since we are considering the case of low carrier concentration. Finally we obtain the following expression for the mobility:

$$\begin{aligned}\mu_{xx} =& -\frac{e_0\beta}{2N_c\hbar^2}\frac{1}{N}\sum_{\mathbf{k},\mathbf{q}}\int_{-\infty}^{\infty}\mathrm{d}t\ \Gamma^x_{\mathbf{k},\mathbf{q}}(t)\times \\ &\times \left\langle c^{\dagger}_{\mathbf{k}}(t) c_{\mathbf{k}} \right\rangle_{H_0} \left\langle c_{\mathbf{q}}(t) c^{\dagger}_{\mathbf{q}} \right\rangle_{H_0},\end{aligned} \tag{39}$$

where

$$\begin{aligned}\Gamma^x_{\mathbf{k},\mathbf{q}}(t) =& \sum_{\mathbf{X},\mathbf{Y},\mathbf{Z}} t_{\mathbf{X}} t_{\mathbf{Y}} X_x Y_x e^{i(\mathbf{q}\mathbf{X}+\mathbf{k}\mathbf{Y}+\mathbf{k}\mathbf{Z}-\mathbf{q}\mathbf{Z})} \times \\ &\times \theta^0_{\mathbf{X}}\theta^0_{\mathbf{Y}}\theta_{\mathbf{X},\mathbf{Y},\mathbf{Z}}(t),\end{aligned} \tag{40}$$

while $\left\langle c^{\dagger}_{\mathbf{k}}(t) c_{\mathbf{k}} \right\rangle_{H_0}$ and $\left\langle c_{\mathbf{q}}(t) c^{\dagger}_{\mathbf{q}} \right\rangle_{H_0}$ are related to the spectral function as

$$\left\langle c^{\dagger}_{\mathbf{k}}(t) c_{\mathbf{k}} \right\rangle_{H_0} = \frac{1}{2\pi}\int_{-\infty}^{\infty}\mathrm{d}\omega\ e^{i\omega t}\frac{\Lambda_{\mathbf{k}}(\omega)}{1+e^{\beta\hbar\omega}} \tag{41}$$

and

$$\left\langle c_{\mathbf{q}}(t) c^{\dagger}_{\mathbf{q}} \right\rangle_{H_0} = \frac{1}{2\pi}\int_{-\infty}^{\infty}\mathrm{d}\omega\ e^{-i\omega t}\Lambda_{\mathbf{q}}(\omega). \tag{42}$$

In Eqs. (41)–(42) we have replaced the bare spectral function with a dressed one in the same spirit of self-consistent approximation used to evaluate the Green's functions.

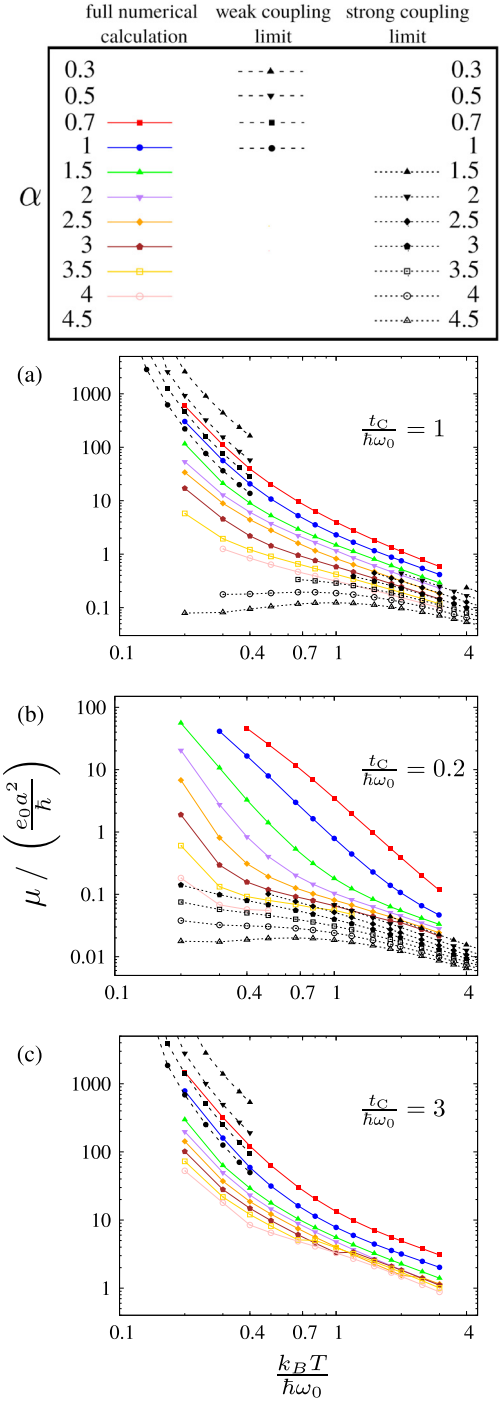

Fig. 5. Temperature dependence of mobility for electron–phonon interaction range $\psi = \frac{\pi}{4}$ and different values of electron–phonon coupling parameter α in the cases when the transfer integral is: (a) $\frac{t_C}{\hbar\omega_0} = 1$; (b) $\frac{t_C}{\hbar\omega_0} = 0.2$; (c) $\frac{t_C}{\hbar\omega_0} = 3$.

Numerical results obtained by evaluating the mobility using Eqs. (39)–(42) are presented in Fig. 5. To gain better understanding of these results, we have also derived analytical or semianalytical results for mobility in the limiting cases of weak and strong electron–phonon interaction for an one dimensional model. These derivations are presented in Appendices A and B. In the case of weak interaction, the mobility can be calculated using Eqs. (A.5) and (A.7), while in the case of strong interaction it is given by Eqs. (B.15) and (B.8). The results in these limiting cases are also presented in Fig. 5. As can be seen from Fig. 5(a), for intermediate adiabaticity ratio $\frac{t_C}{\hbar\omega_0} = 1$, the results for smaller values of α (say $\alpha \leq 1$) converge towards the weak coupling limit for small temperatures, while the results for larger values of α converge towards the strong coupling limit at high temperatures. For small adiabaticity ratio $\frac{t_C}{\hbar\omega_0} = 0.2$, Eqs. (A.5) and (A.7) would yield infinite mobility because bandwidth is narrower than the phonon energy and therefore we do not present the results for weak coupling limit in Fig. 5(b). The high temperature limit results exhibit a reasonably good agreement with numerical results. Slight discrepancy between them originates from the fact that the spectral function contains small peaks at energies $\hbar\omega_0$ below and above the main peak. Consequently, the assumption of a single peaked spectral function given by Eq. (B.1) is not fully justified in this case. On the other hand, for large adiabaticity ratio $\frac{t_C}{\hbar\omega_0} = 3$, we do not present the results for strong coupling limit and high temperatures in Fig. 5(c) because the assumption $\mathrm{Im}\,\Sigma^R(\frac{E-E_F}{\hbar}) \ll \frac{1}{\beta}$ that was used in the derivation of Eqs. (B.15) and (B.8) is not satisfied then. Numerical results for small temperatures converge nicely towards the weak coupling limit in this case.

In Fig. 6, we present the time dependence of the quantity $C(t)$ proportional to the real part of current–current correlation function $\langle j_x(t) j_x(0)\rangle$ for various coupling strengths and temperatures. The shape of this function is also a signature of the transport regime. In the case of weak coupling, $C(t)$ exhibits a relatively slow exponential decay with decay time related to inverse of $-\mathrm{Im}\,\Sigma^R_{\mathbf{k}}\left(\frac{E-E_F}{\hbar}\right)$, see Fig. 6(a), and the carriers are in the band transport regime. When the temperature or coupling strength increase, phononic peaks originating from the $\Gamma^x_{\mathbf{k},\mathbf{q}}(t)$ term start to appear. The appearance of these peaks can already be seen in Fig. 6(a) and (c), while they entirely determine the $C(t)$ graph in Fig. 6(b), (d) and (f) where the carrier exhibits hopping transport. In these figures, the envelope of the peaks exhibits an exponential decay with decay time related to inverse of imaginary part of self-energy. At highest coupling strengths this decay is fast enough to lead to the presence of a single peak in the graph.

We continue the analysis of mobility results with its temperature dependence. The results shown in Fig. 5 demonstrate that the mobility exhibits a monotonous decrease with increasing temperature. At low temperature this dependence is exponential because it is entirely determined by the $\frac{1}{n_0} \approx e^{\frac{\hbar\omega_0}{k_B T}}$ term [as can be seen from the weak coupling limit result given in Eqs. (A.5) and (A.7)]. The decrease of mobility becomes more gradual at high temperatures and is approximately described by a power law $\frac{1}{T^\delta}$ with exponent δ between 1 and 2. The transition between the two regions of temperature dependence is smooth for most values of model parameters. The calculated temperature dependence is slightly discontinuous only in the case of large $\frac{t_C}{\hbar\omega_0}$ ratio and large α, see for example the results for $\alpha \in (2.5 - 4)$ in Fig. 5(c). This occurs in the region where calculated renormalized bandwidth exhibits a sharp transition discussed in Section 3, which can be seen in Fig. 1(b). Slight discontinuity observed in numerical results is therefore most likely a consequence of the fact that the unitary transformation is less successful in this region of parameters.

The dependence of mobility on the value of transfer integral and on electron–phonon coupling strength is in line with expectations — it decreases with increasing the coupling strength and increases with increasing the transfer integral. The details of these dependences can be understood better based on the results for the limiting cases.

It can be seen in Fig. 5 that at low temperatures the dependence of mobility on electron–phonon coupling strength α is more pronounced for smaller $\frac{t_C}{\hbar\omega_0}$ ratio. Namely, the curves at low temperature for different α are separated between each other more for $\frac{t_C}{\hbar\omega_0} = 0.2$ [Fig. 5(b)] than for $\frac{t_C}{\hbar\omega_0} = 1$ [Fig. 5(a)] and $\frac{t_C}{\hbar\omega_0} = 3$ [Fig. 5(c)]. For larger $\frac{t_C}{\hbar\omega_0}$, the dependence of mobility on α in the weak coupling limit is of the $\frac{1}{\alpha^2}$ form [as can be seen from Eqs. (A.5) and (A.7)]. However, for $\frac{t_C}{\hbar\omega_0} < 0.5$, the energy conservation laws imposed by the delta functions in Eq. (A.6) cannot be satisfied because bandwidth is

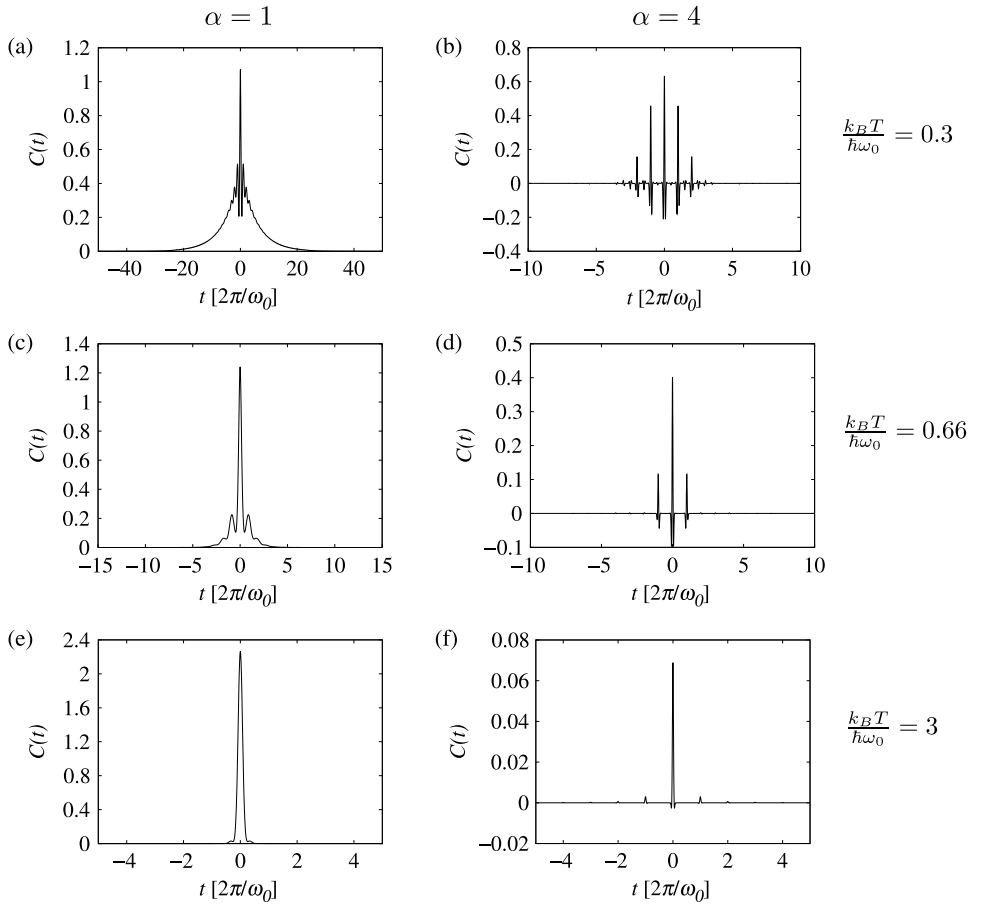

Fig. 6. Time dependence of quantity $C(t)$ proportional to the real part of current–current correlation $\langle j_x(t)j_x(0)\rangle$ for $\frac{t_C}{\hbar\omega_0} = 1$, $\psi = \frac{\pi}{4}$ and: (a) $\alpha = 1$, $\frac{k_BT}{\hbar\omega_0} = 0.3$; (b) $\alpha = 4$, $\frac{k_BT}{\hbar\omega_0} = 0.3$; (c) $\alpha = 1$, $\frac{k_BT}{\hbar\omega_0} = 0.66$; (d) $\alpha = 4$, $\frac{k_BT}{\hbar\omega_0} = 0.66$; (e) $\alpha = 1$, $\frac{k_BT}{\hbar\omega_0} = 3$; (f) $\alpha = 4$, $\frac{k_BT}{\hbar\omega_0} = 3$.

smaller than the phonon energy. One would therefore need to evaluate higher terms to obtain nonzero values of self-energy. These terms give $\frac{1}{\alpha^4}$ rather than $\frac{1}{\alpha^2}$ dependence of the mobility. Consequently, the low temperature dependence of mobility on α is more pronounced for $\frac{t_C}{\hbar\omega_0} < 0.5$. Concerning the dependence on transfer integral, this dependence is roughly of the t_C^2 form in strong coupling region, as expected from Eq. (B.15), while in the weak coupling region it is closer to the t_C dependence, as can be shown from Eq. (A.5).

Next, we discuss the effect of electron–phonon interaction range on mobility. In Fig. 7 we present the temperature dependence of the mobility for different values of electron–phonon interaction range ψ. The results indicate that mobility for the long-range electron–phonon interaction is significantly higher than for a short range one. This result is in-line with the results for renormalized bandwidth that indicate that for the same interaction strength α, short range interaction is more effective in localizing the carrier. The results show that the mobility between the Holstein case ($\psi = 0$) and long-range case ($\psi = \frac{\pi}{4}$ or $\psi = \frac{\pi}{3}$) can vary even by an order of magnitude. This difference originates from the fact that the low momentum electron–phonon coupling contribution is suppressed in the expression for activation energy, $E_a = \frac{1}{2}\hbar\omega_0\sum_{\mathbf{q}} D_{\mathbf{q}}^2(1 - \cos\mathbf{qC})$. Since long-range models have the

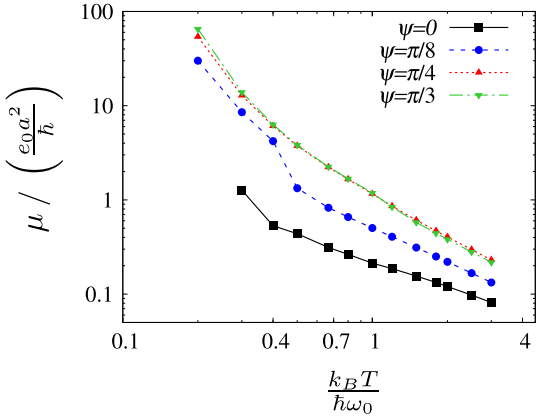

Fig. 7. Temperature dependence of mobility for different values of electron–phonon interaction range ψ for $\alpha = 2$ and $\frac{t_C}{\hbar\omega_0} = 1$.

highest interaction contribution from the low momenta in sharp contrast with the Holstein model which shows no momentum dependence of the coupling coefficients, the mobility is significantly higher in the case of long-range models.

Interestingly, we do not observe thermally activated behavior in any range of investigated parameters. Such behavior also originates from the fact that activation energy E_a is relatively small due to suppression of highest interaction contributions from low momenta by the $(1 - \cos \mathbf{qC})$ factor. We note that the expression for strong coupling limit [Eq. (B.15)] leads to thermally activated behavior in a certain temperature range, as can be seen in Fig. 5(a) and (b). However, this limit does not match the full solution until high temperatures where $k_B T$ is larger than E_a and activation behavior is not observed in the full calculation. As a consequence, in the model with long-range electron–phonon interaction we obtain qualitatively different behavior than in the case of Holstein model where thermally activated behavior sets in for strong electron–phonon coupling and intermediate temperatures, as shown for example in Refs. [30,25].

6. Conclusion

In conclusion, we presented the method for calculation of mobility within lattice models with long-range electron–phonon interaction of Fröhlich type. Numerical results for a wide range of electron–phonon coupling strengths and temperatures were presented, as well as analytical results for limiting cases of weak and strong interaction. Our results indicate that mobility decreases with increasing temperature both in the band transport regime and in the hopping regime, while thermally activated behavior is not observed for any of the model parameters. These results suggest that one cannot make conclusions about charge transport regime based solely on temperature dependence of mobility. We also find that charge carrier mobility increases when the range of electron–phonon interaction is increased.

The results of our study are relevant for qualitative understanding of the mobility in strongly polar inorganic semiconductors where Fröhlich interaction cannot be considered as a perturbation. In the field of organic semiconductors, our model could be of interest in systems containing polar molecules and can possibly be more relevant for description of the system than models with local electron–phonon interaction that are usually applied. Our work opens the way for future studies that would include atomistic details of the material structure and provide a quantitative description of mobility in the materials mentioned.

Acknowledgments

We gratefully acknowledge the support by the Ministry of Education, Science and Technological Development of the Republic of Serbia (Project No. ON171017) and the European Commission under H2020 project VI-SEEM, Grant No. 675121, as well as the contribution of the COST Action MP1406.

Appendix A. Analytical result in the case of weak electron–phonon coupling

In this Appendix, we derive the analytical result for the mobility in the case of weak electron–phonon interaction for an one dimensional model. To obtain $\Gamma^{x}_{\mathbf{k},\mathbf{q}}(t)$, we exploit the fact that in this limit $D_{\mathbf{q}} \to 0$ and consequently $\theta_{\mathbf{X},\mathbf{Y},\mathbf{Z}}(t) \to 1$. By replacing $\theta_{\mathbf{X},\mathbf{Y},\mathbf{Z}}(t) = 1$ in Eq. (40) and using the identities $\frac{1}{N}\sum_{\mathbf{Z}} e^{i(\mathbf{k}-\mathbf{q})\mathbf{Z}} = \delta_{\mathbf{k},\mathbf{q}}$ and $J_{\mathbf{C}} = 2t_{\mathbf{C}}\theta^{0}_{\mathbf{C}}$ we obtain

$$\Gamma^{x}_{\mathbf{k},\mathbf{q}}(t) = -\frac{J^2_{\mathbf{C}} C^2 N}{2}(1-\cos 2\mathbf{q}\mathbf{C})\delta_{\mathbf{k},\mathbf{q}}. \tag{A.1}$$

In the limit of weak electron–phonon interaction, self-energy is small and consequently the spectral function given as:

$$\begin{aligned} &A_{\mathbf{k}}(\omega - \frac{E_F}{\hbar}) = \\ &= \frac{-2\cdot \mathrm{Im}[\,\Sigma^{R}_{\mathbf{k}}(\omega - \frac{E_F}{\hbar})]}{\left(\omega - \frac{E_{\mathbf{k}}}{\hbar} + \mathrm{Re}\,\Sigma^{R}_{\mathbf{k}}(\omega - \frac{E_F}{\hbar})\right)^2 + \left(\mathrm{Im}\,\Sigma^{R}_{\mathbf{k}}(\omega - \frac{E_F}{\hbar})\right)^2} \end{aligned} \tag{A.2}$$

takes the form of a delta function

$$A_{\mathbf{k}}(\omega - \frac{E_F}{\hbar}) \to 2\pi\delta\left(\omega - \frac{E_{\mathbf{k}}}{\hbar}\right), \tag{A.3}$$

while its square takes the form

$$A_{\mathbf{k}}\left(\omega - \frac{E_F}{\hbar}\right)^2 \to \frac{-2\pi}{\mathrm{Im}\,\Sigma^{R}_{\mathrm{k}}\left(\frac{E_{\mathbf{k}}-E_F}{\hbar}\right)}\delta\left(\omega - \frac{E_{\mathbf{k}}}{\hbar}\right). \tag{A.4}$$

After replacing Eqs. (A.1), (41) and (42) into Eq. (39) we obtain

$$\begin{aligned} \mu_{xx} = \frac{e_0 C^2 \beta J^2_{\mathbf{C}}}{4\hbar^2 \sum_{\mathbf{k}} e^{-\beta E_{\mathbf{k}}}} \sum_{\mathbf{k}} (1-\cos 2\mathbf{k}\mathbf{C})\, e^{-\beta E_{\mathbf{k}}} \times \\ \times \frac{-1}{\mathrm{Im}[\,\Sigma^{R}_{\mathbf{k}}(\frac{E_{\mathbf{k}}-E_F}{\hbar})]}. \end{aligned} \tag{A.5}$$

In the limit of weak coupling $D_{\mathbf{q}}$ and $f_{\mathbf{q}}$ are proportional to coupling constant α. By exploiting this fact and keeping the lowest order terms (which are quadratic in α) in expression for self-energy, we obtain that the imaginary part of the self-energy reads

$$\begin{aligned} \mathrm{Im}\left[\Sigma^{R}_{\mathbf{k}}\left(\frac{E_{\mathbf{k}}-E_F}{\hbar}\right)\right] = -\pi \sum_{\mathbf{q}} \hbar\omega_0^2 f^2_{\mathbf{q}} \times \\ \times \left[(n_0+1)\delta\left(E_{\mathbf{k}} - E_{\mathbf{k}-\mathbf{q}} - \hbar\omega_0\right) + \right. \\ \left. + n_0\delta\left(E_{\mathbf{k}} - E_{\mathbf{k}-\mathbf{q}} + \hbar\omega_0\right)\right]. \end{aligned} \tag{A.6}$$

After transformation of the sums in Eq. (A.6) into integrals and evaluation of these integrals we obtain

$$\begin{aligned}\mathrm{Im}\left[\Sigma^R_{\mathbf{k}}\left(\frac{E_{\mathbf{k}}-E_F}{\hbar}\right)\right] = \\ = -\frac{N}{2}\hbar\omega_0^2\sum_{+,-}\left[f^2_{\mathbf{q}_1^{\pm}}\frac{n_0+1}{\sqrt{J_{\mathbf{C}}^2-(J_{\mathbf{C}}\cos\mathbf{kC}+\hbar\omega_0)^2}}+\right. \\ \left.+f^2_{\mathbf{q}_2^{\pm}}\frac{n_0}{\sqrt{J_{\mathbf{C}}^2-(J_{\mathbf{C}}\cos\mathbf{kC}-\hbar\omega_0)^2}}\right],\end{aligned} \tag{A.7}$$

where $q_1^{\pm} = k \mp \frac{1}{C}\arccos\left(\cos kC + \frac{\hbar\omega_0}{J_{\mathbf{C}}}\right)$ and $q_2^{\pm} = k \mp \frac{1}{C}\arccos\left(\cos kC - \frac{\hbar\omega_0}{J_{\mathbf{C}}}\right)$. The first term in Eq. (A.7) should be included only when $E_{\mathbf{k}} > E_{\min} + \hbar\omega_0$, while the second should be included when $E_{\mathbf{k}} < E_{\max} - \hbar\omega_0$, where $E_{\min}$ and $E_{\max}$ are respectively the minimum and maximum renormalized band energy.

Appendix B. Semi-analytical result in the case of strong electron–phonon coupling

In the case of strong electron–phonon interaction, the band is strongly flattened and therefore the relevant Green's functions, self-energies and spectral function do not depend on the wave vector. Therefore the Green's function takes the form

$$G^R\left(\omega-\frac{E_F}{\hbar}\right) = \frac{1}{\omega-\frac{E}{\hbar}-i\cdot\mathrm{Im}\Sigma^R(\frac{E-E_F}{\hbar})}, \tag{B.1}$$

where E is the energy at which the spectral function has a maximum. We also assume that the width of spectral function is rather small in this limit and therefore the value of self-energy at energy E is used in Eq. (B.1). In the time domain Eq. (B.1) reads

$$G^R(t) = -i\Theta(t)\, e^{\mathrm{Im}\Sigma^R\left(\frac{E-E_F}{\hbar}\right)\cdot t} e^{-i\frac{E-E_F}{\hbar}t}. \tag{B.2}$$

Since $f_{\mathbf{q}} \to D_{\mathbf{q}}$ in the limit of strong coupling, the self-energy terms $\Sigma^{(0)}_{\mathbf{k}}(\omega)$ and $\Sigma^{(1)}_{\mathbf{k}}(\omega)$ in Eq. (22) that contain the $f_{\mathbf{q}} - D_{\mathbf{q}}$ term vanish and the self-energy is determined by the $\Sigma^{(2)}_{\mathbf{k}}(\omega)$ term defined in Eq. (25). From Eqs. (25) and (27) and the identity $\frac{1}{N}\sum_{\mathbf{q}} e^{i\mathbf{q}(\mathbf{Z}-\mathbf{X})} = \delta_{\mathbf{Z},\mathbf{X}}$ we obtain

$$\begin{aligned}\Sigma^R\left(\omega-\frac{E_F}{\hbar}\right) = \frac{1}{\hbar^2}\int_{-\infty}^{\infty}\mathrm{d}t\, e^{i\left(\omega-\frac{E_F}{\hbar}\right)t}G^R(t)\times \\ \times\sum_{\mathbf{X},\mathbf{Y}} t_{\mathbf{X}}t_{\mathbf{Y}}e^{i\mathbf{k}(\mathbf{X}+\mathbf{Y})}e^{-2\sum_{\mathbf{q}}D_{\mathbf{q}}^2(1-\cos\mathbf{qX})(2n_0+1)}\times \\ \times\left(e^{\sum_{\mathbf{q}}D_{\mathbf{q}}^2\left[(n_0+1)e^{-i\omega_0 t}+n_0e^{i\omega_0 t}\right]\left[1-e^{i\mathbf{qX}}-e^{i\mathbf{qY}}+e^{i\mathbf{q}(\mathbf{X}+\mathbf{Y})}\right]}-1\right).\end{aligned} \tag{B.3}$$

Since $D_{\mathbf{q}}$ is large in this limit, the exponential term will determine the value of the term in the last line of Eq. (B.3). The terms with $\mathbf{X} = -\mathbf{Y}$ in Eq. (B.3) make a much larger contribution than the ones having $\mathbf{X} = \mathbf{Y}$ because of a larger factor in the exponent in the last line of Eq. (B.3). By keeping only the terms with $\mathbf{X} = -\mathbf{Y}$ we find

$$\Sigma^R\left(\omega-\frac{E_F}{\hbar}\right) = \frac{2t_{\mathbf{C}}^2}{\hbar^2}\int_{-\infty}^{\infty}\mathrm{d}t\, e^{i\left(\omega-\frac{E_F}{\hbar}\right)t}G^R(t)g(t), \tag{B.4}$$

where

$$g(t) = e^{-4\frac{E_a}{\hbar\omega_0}\left[2n_0+1-(n_0+1)e^{-i\omega_0 t}-n_0e^{i\omega_0 t}\right]}, \tag{B.5}$$

with

$$E_a = \frac{1}{2}\hbar\omega_0 \sum_{\mathbf{q}} D_{\mathbf{q}}^2 \left(1 - \cos \mathbf{qC}\right). \tag{B.6}$$

Eq. (B.4) can be further simplified by taking into account that the function $g(t)$ is periodic and that in the strong coupling limit it peaks prominently at $t = mT_0$ (where m is integer and $T_0 = \frac{2\pi}{\omega_0}$), reaching its maximum value of 1. In comparison to this, the retarded Green's function decays as $e^{\mathrm{Im}\Sigma^R \cdot t}$. This decay is slow because self-energy is not large since the unitary transformation nearly diagonalizes the Hamiltonian. Consequently, the Green's function varies slowly on the timescales on which g varies, so it can be approximated by its value in points $t = mT_0$ for the application of the mean value theorem. By exploiting this fact, as well as periodicity of the function g, one obtains:

$$\begin{aligned}\Sigma^R\left(\omega - \frac{E_F}{\hbar}\right) = &\frac{2t_{\mathbf{C}}^2}{\hbar^2}\Bigg[\gamma_1 G^R(0) + \\ &+ \gamma_2 \sum_{m=1}^{\infty} e^{i\left(\omega - \frac{E_F}{\hbar}\right)mT_0} G^R(mT_0)\Bigg]\end{aligned} \tag{B.7}$$

where $\gamma_1 = \int_0^{\frac{T_0}{2}} \mathrm{d}t\, g(t)$ and $\gamma_2 = \int_{-\frac{T_0}{2}}^{\frac{T_0}{2}} \mathrm{d}t\, g(t)$. By replacing $\omega = \frac{E}{\hbar}$ in Eq. (B.7) we obtain

$$\mathrm{Im}\Sigma^R\left(\frac{E - E_F}{\hbar}\right) = -\frac{2t_{\mathbf{C}}^2}{\hbar^2}\left[\mathrm{Re}\gamma_1 + \mathrm{Re}\gamma_2 \frac{e^{\mathrm{Im}\Sigma^R\left(\frac{E-E_F}{\hbar}\right)\cdot T_0}}{1 - e^{\mathrm{Im}\Sigma^R\left(\frac{E-E_F}{\hbar}\right)\cdot T_0}}\right]. \tag{B.8}$$

Eq. (B.8) contains a single unknown $\mathrm{Im}\Sigma^R\left(\frac{E-E_F}{\hbar}\right)$. Although it must be solved numerically, the value of $\mathrm{Im}\Sigma^R\left(\frac{E-E_F}{\hbar}\right)$ can be found very accurately.

To obtain the mobility, we substitute the expression for the spectral function

$$\Lambda\left(\omega - \frac{E_F}{\hbar}\right) = \frac{-2 \cdot \mathrm{Im}\Sigma^R\left(\frac{E-E_F}{\hbar}\right)}{\left(\omega - \frac{E}{\hbar}\right)^2 + \left(\mathrm{Im}\Sigma^R\left(\frac{E-E_F}{\hbar}\right)\right)^2} \tag{B.9}$$

into Eqs. (41)–(42). In Eq. (41) we replace the Fermi–Dirac term $1 + e^{\beta(\hbar\omega - E_F)}$ with its value at $\omega = \frac{E}{\hbar}$ since it varies much slower than the spectral function when the condition $\mathrm{Im}\Sigma^R(\frac{E-E_F}{\hbar}) \ll \frac{1}{\beta}$ is satisfied. After performing the integration in Eqs. (41)–(42) we obtain

$$\left\langle c^\dagger(t)\, c\right\rangle \cdot \left\langle c\, c^\dagger(t)\right\rangle = \frac{e^{2\cdot\mathrm{Im}\Sigma^R\left(\frac{E-E_F}{\hbar}\right)\cdot|t|}}{1 + e^{\beta(E-E_F)}}, \tag{B.10}$$

where the momentum indices have been dropped because the momentum dependence is lost in this limit.

Using the identity

$$\frac{1}{N^2}\sum_{\mathbf{k},\mathbf{q}} e^{i\mathbf{q}\cdot(\mathbf{X}-\mathbf{Z})} e^{i\mathbf{k}\cdot(\mathbf{Y}+\mathbf{Z})} = \delta_{\mathbf{X},\mathbf{Z}} \cdot \delta_{\mathbf{Y},-\mathbf{Z}} \tag{B.11}$$

and taking into account that from previous definition of $g(t)$ the following identity holds when $\mathbf{X} = -\mathbf{Y} = \mathbf{Z}$:

$$g(t) = \theta_{\mathbf{X}}^0 \theta_{\mathbf{Y}}^0 \theta_{\mathbf{X},\mathbf{Y},\mathbf{Z}}(t) \tag{B.12}$$

we find

$$\frac{1}{N^2}\sum_{\mathbf{k},\mathbf{q}} \Gamma_{\mathbf{k},\mathbf{q}}^x(t) = -2t_{\mathbf{C}}^2 C^2 g(t). \tag{B.13}$$

From Eqs. (39), (B.11), (B.13) one obtains the mobility

$$\mu_{xx} = \frac{e_0 \beta t_C^2 C^2}{\hbar^2} \int_{-\infty}^{\infty} \mathrm{d}t \; g(t) \, e^{2 \cdot \mathrm{Im}\Sigma^R\left(\frac{E-E_F}{\hbar}\right) \cdot |t|}. \tag{B.14}$$

Using the same mean value approximation as for the self-energy in (B.7), we finally obtain:

$$\mu_{xx} = \frac{e_0 \beta t_C^2 C^2}{\hbar^2} \gamma_2 \left[1 + 2 \cdot \frac{e^{2 \cdot \mathrm{Im}\Sigma^R\left(\frac{E-E_F}{\hbar}\right) \cdot T_0}}{1 - e^{2 \cdot \mathrm{Im}\Sigma^R\left(\frac{E-E_F}{\hbar}\right) \cdot T_0}} \right]. \tag{B.15}$$

Expressions (B.15) and (B.8) completely determine the mobility in the strong coupling approximation.

We note that well known Marcus formula is obtained by exploiting the short-time approximation [19] $e^{\pm i\omega_0 t} = 1 \pm i\omega_0 t - \frac{1}{2}\omega_0^2 t^2$ and high temperature approximation $k_B T \gg \hbar\omega_0$, i.e. $n_0 = \frac{k_B T}{\hbar\omega_0}$. Using the short-time approximation for $g(t)$ in Eq. (B.14) and taking into account that for short times the exponential term in that equation is 1, one obtains

$$\mu_{xx} = \frac{e_0 t_C^2 C^2}{2\hbar (k_B T)^{3/2}} \sqrt{\frac{\pi}{E_a}} e^{-\frac{E_a}{k_B T}}. \tag{B.16}$$

References

[1] B.K. Ridley, Quantum Processes in Semiconductors, Clarendon Press, Oxford, 1999.
[2] M. Lundstrom, Fundamentals of Carrier Transport, Cambridge University Press, Cambridge, 2000.
[3] N.W. Ashcroft, N.D. Mermin, Solid State Physics, Harcourt, Orlando, 1976.
[4] F. Giustino, Rev. Modern Phys. 89 (2017) 015003.
[5] B. Liao, J. Zhou, B. Qiu, M.S. Dresselhaus, G. Chen, Phys. Rev. B 91 (2015) 235419.
[6] T. Gunst, T. Markussen, K. Stokbro, M. Brandbyge, Phys. Rev. B 93 (2016) 035414.
[7] J.-J. Zhou, M. Bernardi, Phys. Rev. B 94 (2016) 201201.
[8] C.-H. Park, N. Bonini, T. Sohier, G. Samsonidze, B. Kozinsky, M. Calandra, F. Mauri, N. Marzari, Nano Lett. 14 (2014) 1113.
[9] N. Sule, I. Knezevic, J. Appl. Phys. 112 (2012) 053702.
[10] W. Li, Phys. Rev. B 92 (2015) 075405.
[11] F. Giustino, M.L. Cohen, S.G. Louie, Phys. Rev. B 76 (2007) 165108.
[12] J. Noffsinger, F. Giustino, B.D. Malone, C.-H. Park, S.G. Louie, M.L. Cohen, Comput. Phys. Comm. 181 (2010) 2140.
[13] C. Verdi, F. Giustino, Phys. Rev. Lett. 115 (2015) 176401.
[14] J. Sjakste, N. Vast, M. Calandra, F. Mauri, Phys. Rev. B 92 (2015) 054307.
[15] V. Coropceanu, J. Cornil, D.A. da Silva Filho, Y. Olivier, R. Silbey, J.-L. Bredas, Chem. Rev. 107 (2007) 926.
[16] R.A. Marcus, Rev. Modern Phys. 65 (1993) 599.
[17] L. Wang, G. Nan, X. Yang, Q. Peng, Q. Li, Z. Shuai, Chem. Soc. Rev. 39 (2010) 423.
[18] S.H. Lin, C.H. Chang, K.K. Liang, R. Chang, Y.J. Shiu, J.M. Zhang, T.-S. Yang, M. Hayashi, F.C. Hsu, Ultrafast Dynamics and Spectroscopy of Bacterial Photosynthetic Reaction Centers, in: Advances in Chemical Physics, John Wiley and Sons, Inc., 2002, pp. 1–88.
[19] G. Nan, X. Yang, L. Wang, Z. Shuai, Y. Zhao, Phys. Rev. B 79 (2009) 115203.
[20] N. Prodanović, N. Vukmirović, Z. Ikonić, P. Harrison, D. Indjin, J. Phys. Chem. Lett. 5 (2014) 1335.
[21] J.T. Devreese, A.S. Alexandrov, Rep. Progr. Phys. 72 (2009) 066501.
[22] S.N. Klimin, J. Tempere, J.T. Devreese, Phys. Rev. B 94 (2016) 125206.
[23] J. Vlietinck, W. Casteels, K.V. Houcke, J. Tempere, J. Ryckebusch, J.T. Devreese, New J. Phys. 17 (2015) 033023.
[24] F. Ortmann, S. Roche, Phys. Rev. B 84 (2011) 180302(R).
[25] F. Ortmann, F. Bechstedt, K. Hannewald, Phys. Rev. B 79 (2009) 235206.
[26] Y.-C. Cheng, R.J. Silbey, J. Chem. Phys. 128 (2008) 114713.
[27] V.M. Stojanović, P.A. Bobbert, M.A.J. Michels, Phys. Rev. B 69 (2004) 144302.
[28] K. Hannewald, V.M. Stojanović, J.M.T. Schellekens, P.A. Bobbert, G. Kresse, J. Hafner, Phys. Rev. B 69 (2004) 075211.
[29] L.J. Wang, Q. Peng, Q.K. Li, Z. Shuai, J. Chem. Phys. 127 (2007) 044506.
[30] A.S. Mishchenko, N. Nagaosa, G. De Filippis, A. de Candia, V. Cataudella, Phys. Rev. Lett. 114 (2015) 146401.
[31] G. De Filippis, V. Cataudella, A.S. Mishchenko, N. Nagaosa, A. Fierro, A. de Candia, Phys. Rev. Lett. 114 (2015) 086601.
[32] T. Holstein, Ann. Phys. 8 (1959) 343.
[33] A.S. Alexandrov, P.E. Kornilovitch, Phys. Rev. Lett. 82 (1999) 807.
[34] I.G. Lang, Y.A. Firsov, Sov. Phys.—JETP 16 (1963) 1301.
[35] A. Isihara, J. Phys. A Gen. Phys. 1 (1968) 539.
[36] B. Gerlach, H. Löwen, Phys. Rev. B 35 (1987) 4291.

[37] D.W. Brown, K. Lindenberg, Y. Zhao, J. Chem. Phys. 107 (1997) 3179.
[38] A.H. Romero, D.W. Brown, K. Lindenberg, Phys. Lett. A 266 (2000) 414.
[39] P.E. Spencer, J.H. Samson, P.E. Kornilovitch, A.S. Alexandrov, Phys. Rev. B 71 (2005) 184310.
[40] G. Mahan, Many-Particle Physics, Kluwer Academic, New York, 2000.
[41] Q. Liu, Phys. Lett. A 376 (2012) 1219.
[42] M. Berciu, G.A. Sawatzky, Europhys. Lett. 81 (2008) 57008.